First Order Thermal Model of the Navy integrated Power Electronics Building Block

by

Ethan Lietch

Submitted to the
Department of Mechanical Engineering
in Partial Fulfillment of the Requirements for the Degree of

Bachelor of Science in Mechanical Engineering

at the Massachusetts Institute of Technology

May 6, 2022

© Massachusetts Institute of Technology 2022. All rights reserved.

Signature of Author:	
	Department of Mechanical Engineering
	May 6, 2021
Certified by:	
-	Julie Chalfant
	Research Scientist
	Thesis Supervisor
Certified by:	
•	Chryssostomos Chryssostomidis
	Professor of Mechanical and Ocean Engineering
	Thesis Supervisor
Accepted by:	
	Kenneth Kamrin
	Associate Professor of Mechanical Engineering

Undergraduate Officer

First Order Thermal Model of the Navy integrated Power Electronics Building Block

by

Ethan Lietch

Submitted to the Department of Mechanical Engineering on May 6, 2022, in Partial Fulfillment of the Requirements for the Degree of

Bachelor of Science in Mechanical Engineering

ABSTRACT

To accomplish the United States Navy's goal of developing a fully electric warship, it is essential to cool critical electronic components within the Navy integrated Power Electronics Building Block (iPEBB) for it to function at its full capacity. The current study develops a first order analytical understanding of the most prolific heat transfer modes within the iPEBB and identifies critical constraints for the design of future cooling systems. The main heat loads within the iPEBB are the rows of MOSFET switches generating 4752 W of waste heat and the transformer which generates 858 W through the outer protective wall. The analysis presented in this thesis defines the critical temperatures and heat fluxes of the critical heat generating sources and can be used as a benchmark for future thermal cooling design.

Thesis Supervisor: Julie Chalfant

Title: Research Scientist

Thesis Supervisor: Chryssostomos Chryssostomidis Title: Professor of Mechanical and Ocean Engineering

Table of Contents

ABSTRACT	2
Acknowledgements	4
I. Introduction	5
II. Background	6
A. iPEBB	6
B. SiC MOSFET Bridges	8
C. Transformer	9
D. Common Substrate	10
E. Material Properties	11
III. Thermal Model	12
A. Conduction Modes Within the Substrate	12
B. Thermal Model of Transformer	16
C. Thermal Model of MOSFETs	31
a. Heat Spreading Experimentation	34
b. iPEBB MOSFET Heat Spreading Analysis	39
D. Conclusions	42
References	44
Appendix	45
Core Biot analysis:	45
Temperature Profile of Transformer Core:	46
Temperature Profile of Transformer Substrate:	47

List of Figures

Figure 1: iPEBB Visualization	7
Figure 2: Heat Generating Elements in the iPEBB.	8
Figure 3: MOSFET Row Arrangement	9
Figure 4: CAD Rendition of Transformer	10
Figure 5: Substrate Layers	11
Figure 6: Conduction Modes through Substrate	12
Figure 7: Lateral Thermal Resistance Network in Substrate	13
Figure 8:Thermal Resistance Network in Substrate Z Direction	14
Figure 9: Area of Thermal Resistance Network in Substrate Z Direction	
Figure 10: Transformer Planes of Symmetry	17
Figure 11: Copper Wire and Transformer System	18
Figure 12: Annulus Representation of Coils	19
Figure 13: Simplified Transformer Coil Orientation	21
Figure 14: Transformer Cylinder Control Volume	21
Figure 15: Geometry of Transformer Core	24
Figure 16: Thermal Assumptions in Transformer Core	25
Figure 17: Control Volume of Thermal Core.	26
Figure 18: Temperature Profile Through Transformer	31
Figure 19: Heat Flow Through Multi-Substrate Wall	33
Figure 20: Heat Spreading Experiment Set-Up	34
Figure 21: Heat Spreading Angle Diagram	37
Figure 22: Thermal Overlap of Heat Spreading Angle	40
List of Tables	
Table 1: Material Properties of iPEBB	
Table 2: Material Properties of Experiment	35

Acknowledgements

I would like to take the time to give thanks to Professor Chryssostomidis and Dr. Chalfant for their continuous guidance and support throughout the entire analysis process and the writing of this thesis. I appreciate their dedication to this project and their encouragement when I felt overwhelmed during the semester. I would also like to thank Joushua Padilla for his outstanding ability to motivate and challenge me to solve difficult problems, and I am incredibly thankful to have him as a mentor and as a friend. I also would like to thank our sponsors Kelly Cooper and L.J. Petersen from the Office of Naval Research, who sponsored our research under grants ONR N00014-16-1-2956 and N00014-16-1-2356.

I. Introduction

Fully electric warships are incredibly beneficial to the United States Navy from a logistical and safety perspective. By electrifying ships, the Navy can power multiple systems and has the flexibility to control and direct energy where it is needed [1]. This is a significant development because the ship can use one source of power for all its operation systems including its propulsion. If the technology is redundant and simple to operate, the maintenance and manpower demands of the ship are reduced [2]. This suggests that crew sizes can decrease, and fewer sailors could be sent into combat. Due to these potential benefits, the United States Navy is currently pursuing their goal of electrifying warships through a five-year program to develop the Power Electronic Power Distribution Systems (PEPDS). PEPDS is a universal solution to power distribution because it can perform with AC, DC, or both signals; this is revolutionary for electrifying warships because the current Integrated Power and Energy System (IPES) can only use AC or DC [3]. PEPDS has the flexibility to provide any kind of electrical load or function to the ship, and it is a breakthrough because the ship only relies on the PEPDS to provide for nearly all its energy needs. Thus, the total energy system of the ship is consolidated into a single system.

The heart of the PEPDS system lies within the power corridor, which is the space within the ship designated to house all elements of the power distribution system of an all-electric ship apart from power generation and power usage [4]. The power corridor is a reserved space early in the ship design that is adaptive and fully customizable. More importantly, this defined and isolated space in a heavily reinforced location within the ship, thus improving sailor safety by reducing unintended exposures to electrical equipment [3]. The power corridor is incredibly effective for the PEPDS system because it consists of modular universal power converters known as the Navy integrated Power Electronics Building Block (iPEBB). The iPEBBs are extremely useful for the resilience of the power system because each unit can be connected in series or parallel in a manner that is designed for soft power degradation. Therefore, if a component fails, the capability is still functional at a reduced level [3]. The iPEBB design is portable and easily replaceable, so the crew can easily swap out damaged iPEBBs but leave the surrounding system in place if the equipment is still viable [5]. This drastically reduces the system complexity because the least replaceable component of the power system can adapt to any use case in the power corridor. Furthermore, due to the portability and relative ease to connect to the system, the iPEBBs can be manufactured and tested in a clean factory setting off-hull which reduces costs and improves reliability of the system [5].

Although the iPEBB system is an effective solution to the electrification of naval ships from an electrical engineering aspect, there are significant thermal challenges that need to be addressed before the system can be employed. Firstly, liquid connections are not allowed within the iPEBB, meaning that direct liquid cooling methods are strictly prohibited [6]. This constraint is in place to ensure that the process to insert and remove the iPEBB is simple, and to additionally protect the iPEBBs from water damage. Although this decision has a strong logistical benefit, it greatly increases the complexity of the cooling problem. Due to the portability requirement of the iPEBBs, large-finned air heat exchangers are not an adequate solution because they are simply not

compact nor robust; however, previous iterations of the PEBB design utilized cooling methods achieved with a finned aluminum heat sink coupled with a robust air forced convection system that removes heat from critical producing elements [6].

The present study intends to first create a first order analytical model of the heat transfer network to understand the magnitude of the heat flux exiting the iPEBB. At very high heat fluxes, water cooling is necessary to dissipate waste heat, but further examination is necessary to establish if water cooling is necessary for the iPEBB.

II. Background

It is essential to clearly define the scope of the heat transfer problem before the analytical modeling process. Below, we will develop all relevant elements that contribute to the heat transfer circuit including the overall layout of the iPEBB, the various components within the iPEBB, and the failure modes of the critical electrical components.

A. iPEBB

The iPEBB is designed to be easily transportable through narrow passageways and ladders within the ship, which leads to a necessary weight requirement of less than 35lbs. This is a significant restriction because the current weight of the iPEBB V3 is 31lbs, thus severely limiting the scope of viable cooling options. To meet the weight requirement, the cooling system must be small and compact (under 2kg); if this is not possible, the iPEBB would likely have to shed weight to meet its target value. A possible solution to the weight constraint is to limit cooling mechanisms directly to critical areas that generate heat and consequently ignore the areas unlikely to be affected by the heat generation within the iPEBB. Additionally, the current Navy iPEBB V3 is currently designed to be 300mm x 550mm x 100mm (Figure 1). It is important to note that the dimensional requirements are not strictly constrained, and the shape of the iPEBB could change in future iterations. Additionally, the iPEBB dimensions do not include any supplemental parts needed by the cooling system; the size of the cooling system is not rigidly defined; rather, the volume of the cooling mechanism needs to be reasonable compared to the iPEBB.

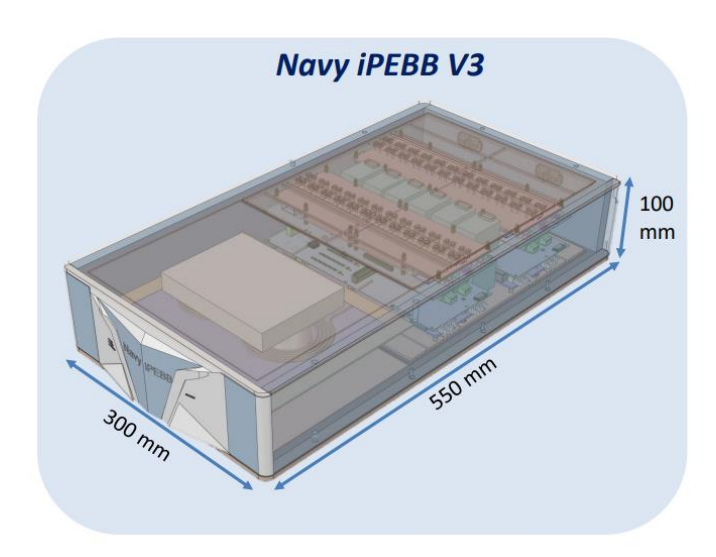


Figure 1: The image above displays the dimensions of the Navy iPEBB V3. It is important to note that the iPEBB is designed to be a rectangular shape and depicted with outer substrate walls constraining the inner electrical components. This modular design allows the iPEBBs to be easily ordered in expandible, compact grids within the power corridor of the ship [7].

As shown above, the iPEBB is an enclosed box with electrical components that generate heat as they perform various processes to supply power to different operations within the ship. This is problematic because the heat generated within the box can only transfer out into the environment through conduction, and a cooling mechanism is essential to increase the rate of heat transfer out of the system. If heat cannot transfer out of the iPEBB efficiently, the iPEBB must decrease its operational power or risk damaging components within the shell. To stay in operation, the cooling system must control the temperature of the most critical heat producing elements of the iPEBB: the MOSFET switches and the transformer (Figure 2). These elements produce virtually all the waste heat in the iPEBB and will subsequently have the highest temperatures within the iPEBB.

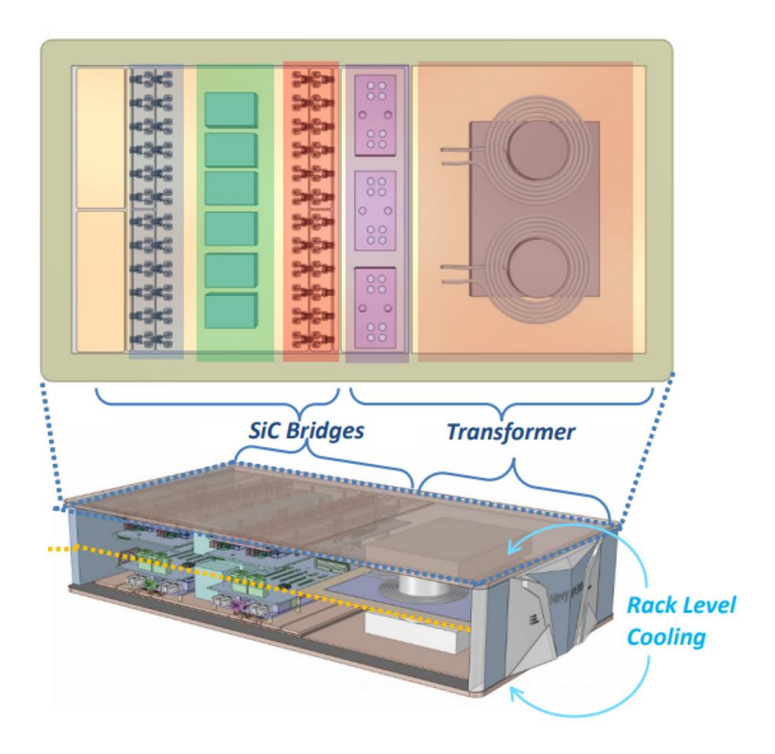


Figure 2: The image above depicts the critical heat generation elements within the iPEBB. The MOSFET switches are depicted in the blue and red regions in the image. It is important to note that the image above only displays the cross-sectional view of the top shell of the iPEBB, but there is a mirrored image on the bottom shell. This means that there is a total of four rows of switches within the iPEBB. Moreover, there is only one transformer located in the iPEBB. Figure 2 also presents the top and bottom shell surfaces as the location for Rack Level Cooling; the cooling method will be placed on these surfaces to increase the heat flux near the MOSFET switches and the transformer [7].

By imposing a rack level cooling design on the top and bottom of the iPEBB, we can focus on cooling the critical concentrated heat loads generated by the rows of switches and the transformer.

B. SiC MOSFET Bridges

The first critical element of the iPEBB is the SiC MOSFET bridges that are located inside the top and bottom shells. Both top and bottom substrates have two rows of switches consisting of 24 MOSFETs in each row, for a total of 48 switches per substrate and 96 switches in the entire iPEBB (Figure 3).

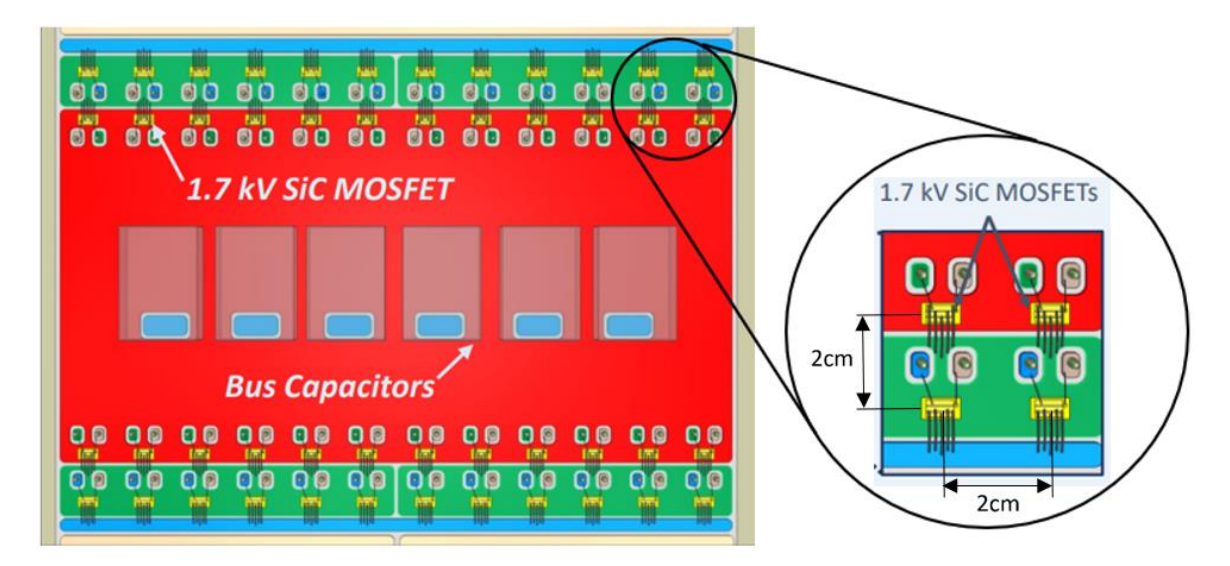


Figure 3: This image shows the arrangement of two rows of SiC MOSFETs on one substrate. It is important to note that the switches are in very near proximity to one another which can lead to a significant heat concentration that will potentially deteriorate the electrical capability of the switches. As shown in the figure, the center of each switch is spaced 2cm apart, which will lead to heat spreading effects between the switches [7].

Each MOSFET has a square prism shape with a thickness of 1mm and a side length of 1cm, and the total MOSFET system has two components that lead to heat generation: conduction losses of 3066W and switching losses of 1686W. The conduction losses are inherent to the system when power is supplied, but the switching losses only occur when the SiC MOSFETS are actively switching. Since this study intends to model and design for the worst-case scenario, it is assumed that both losses are present in the iPEBB and distributed between the switches. With this assumption, the iPEBB endures a total of 4752W in total losses throughout the switching system, with each MOSFET producing 49.5W of waste heat.

The MOSFETs are the most challenging problem from a thermal engineering perspective because they are placed very close to one another which severely inhibits heat spreading in the planar directions. This design essentially creates a giant heat source that will need additional cooling treatments to ensure the equipment is fully operational. Furthermore, SiC MOSFETs generally have operational temperatures ranging between 150 to 200 degrees Celsius; thus, the current study will proceed with the goal of keeping each switch below 150 degrees Celsius. This is essential not only in the design for the extreme scenarios, but also because MOSFETs with lower operating temperatures are much less expensive and desired by the Navy.

C. Transformer

The second critical heat generation element is the singular high frequency transformer and is located opposite of the SiC MOSFET bridges within the iPEBB. Although the current transformer is smaller and more compact than previous designs (dimensioned as $0.102 \text{m x} \ 0.305 \text{m} \text{m} \times 0.254 \text{m}$), it still limits the size of the iPEBB in the vertical direction because it is the largest

element in the system. The transformer consists of two main elements that dissipate heat (Figure 4): the ferrite core (300W) and the copper coils (800W).

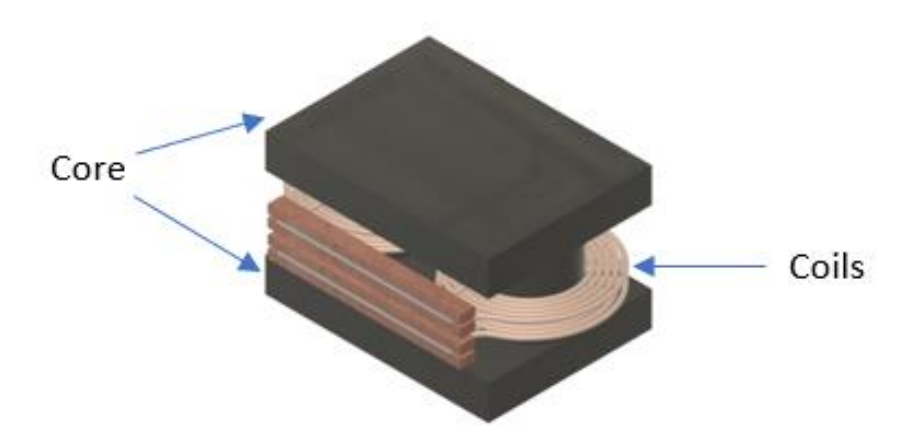


Figure 4: The image shown is a CAD rendition of the current transformer prototype (Rev2). Notably, the core of the transformer consists of two rectangular prisms with a thickness of 0.025m, and two cylinders with a length of 0.051m and a diameter of 0.127m. The coils wrapped around the core cylinders consist of 4000 44 AWG copper wires that can be approximated by a singular wire being size 6 AWG with an outside diameter of 4.064mm. As depicted in the picture above, the coils and core have complex thermal interactions due to the geometry of the transformer system [8].

The copper wires are not a thermal concern since they are functional up until their melting point of 1,085 degrees Celsius, although the current study imposes a maximum operating limit on the copper wires as 250 degrees Celsius due to melting concerns of insulation materials and plastic around the copper wires. The core is also at risk of overheating with the current Rev2 prototype core being Ferrite N49 which has a Curie temperature of 240 degrees Celsius; if the core increases above the Curie temperature, the Ferrite N49 will lose its magnetic properties. The current study intends to design a thermal model with the Curie temperature as the maximum operating temperature of the transformer, but it is noted that most transformers are regulated to run well below the Curie temperature (usually 100-200 degrees Celsius) because there is a known performance loss at high temperatures.

D. Common Substrate

The iPEBB walls are made from a common substrate that consists of multiple layers of copper and polyimide (Figure 5). The common substrate functions as a protective barrier for electrical components in the iPEBB with its mechanical strength and voltage isolation.

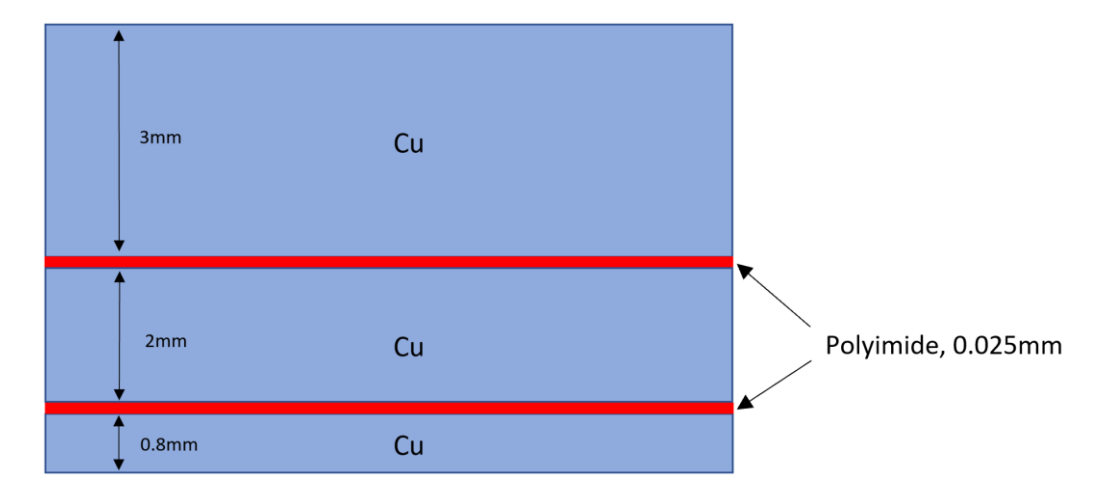


Figure 5: The diagram above shows the different layers of the common substrate, with the 3mm thick copper layer on the inside surface of the iPEBB, and the total thickness is 5.8mm. The common substrate is critical to the thermal cooling problem because the waste heat from the array of switches and the transformer will conduct through the common substrate and out into the ambient air in the power corridor.

It is assumed that the MOSFET switches and the transformer are rigidly attached to the inside surface of the common substrate, and the cooling mechanism is rigidly attached to the outside surface of the common substrate to drive conductive cooling. Notably, polyimide has a thermal conductivity of 0.12 W/m-K which is significantly smaller than copper (398 W/m-k), meaning that most of the thermal resistance within the common substrate is due to the thin polyimide layers.

E. Material Properties

The following section provides a summary of the materials of critical elements to the heat transfer system and their thermal properties:

Table 1

System	Material	Thermal	Heat Generation from
	Conductivity		Associated Part
		[W/m-K]	[W]
SiC MOSFET	Silicon-Carbon	77.5	49.5 (per MOSFET)
Transformer (Core)	Iron	76.2	300
Transformer (Coil)	Copper	398	800
Common Substrate	Polyimide	0.12	N/A
Common Substrate	Copper	398	N/A

III. Thermal Model

Now that the materials and general layout of the iPEBB are understood, this section intends to methodically analyze elements within the heat transfer system to accurately depict the heat transfer network. This process relies on common engineering assumptions to simplify a complex thermal problem into smaller, solvable parts that reflect the critical modes of heat transfer. This process is crucial in analysis because it allows minor thermal interactions to be neglected, yet it predicts the broader system behavior with a high degree of accuracy.

A. Conduction Modes Within the Substrate

The first step in simplifying the heat transfer network is to understand how heat transfers through the substrate walls (Figure 6). This is an important first step because it determines if the heat sources (the switches and the transformer) have any thermal interactions via conduction through the substrate walls. Additionally, if the thermal resistance is much higher in the lateral direction, the substrate could simplify using the thin-wall assumption and reduce the problem to one dimension within the substrate.

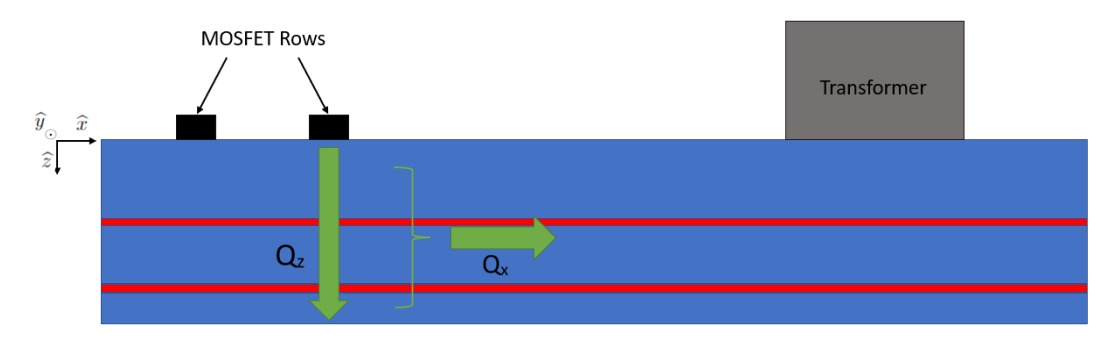


Figure 6: The diagram above (not drawn to scale) shows two conduction heat transfer modes (depicted as green arrows) within the substrate walls. Additionally, there is a heat flux in the y direction not shown in the figure. The heat flux in the y direction is equivalent to the heat flux in the x direction because both fluxes travel through identical resistance networks. However, the thermal resistance in the z direction is different due to the geometry of the substrate. In the following analysis, the thermal resistance in the z direction will be directly compared to the thermal resistance in the x and y directions to determine the dominant mode of heat transfer.

The first step in the process of analyzing conduction resistances is to determine the resistance circuits. For the substrate in the z direction and in the x direction. In the following analysis, it is assumed that the thermal properties in the y direction are identical to the x direction due to symmetry arguments. The thermal circuit in the x direction is as follows in Figure 7:

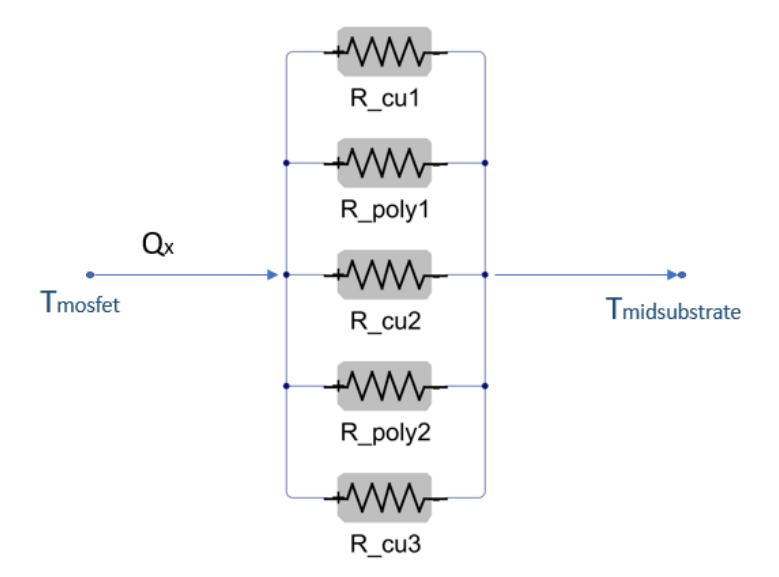


Figure 7: The picture above shows the thermal resistance network through the x direction (lateral through the iPEBB substrate). It is important to note that the final temperature ($T_{midsubstrate}$) represents the steady temperature in the middle of the substrate wall.

The heat transfer through the lateral direction passes through five conductive resistors in parallel. Simplifying the problem, the equivalent resistance in the x direction is shown below:

$$\frac{1}{R_x} = \frac{1}{R_{cu1}} + \frac{1}{R_{p1}} + \frac{1}{R_{cu2}} + \frac{1}{R_{p2}} + \frac{1}{R_{cu3}}$$
 (1)

$$\frac{1}{R_x} = \frac{1}{R_{cu}} + \frac{1}{R_p} \tag{2}$$

$$\frac{1}{R_x} = \frac{K_{cu} * A_{cu}}{L} + \frac{K_p * A_p}{L} \tag{3}$$

The equivalent resistance in the x direction is denoted as R_x . Additionally, since each layer in the substrate has the same length, the resistance network can be reduced to the parallel system of polyimide and copper (Eq. 2). The terms A_{cu} (1.7*10⁻³ m²) and A_p (1.5*10⁻⁵ m²) denote the cross-sectional areas of the copper layer and the polyimide layer respectively. The L term refers to the length of the substrate in the x direction. For this analysis we will look at two cases: half of the distance between the two rows of switches (L=0.0393m) and half of the distance between the transformer and the nearest row of switches (L=0.688m). Solving with known constants in Eq. 3, we find the resistances:

The lateral conduction resistance between the two MOSFET rows is shown below:

$$R_{x,Mosfet-Mosfet} = 0.0567 \frac{K}{W}$$

Furthermore, the lateral conduction resistance between the MOSFET row and the transformer is shown below:

$$R_{x,Mosfet-Transformer} = 0.0993 \frac{K}{W}$$

Now that the conductive resistances are found in the x direction, the same process is applied to the z direction (Figure 8):

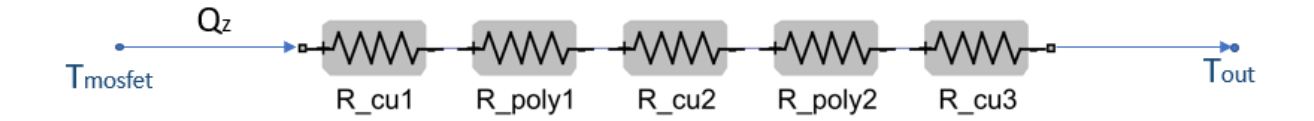


Figure 8: The diagram above depicts the thermal circuit in the z direction. This circuit is significantly different from the one shown in Figure 7 because heat travels through every layer of the substrate in series, thus making the total equivalent resistance greater than the parallel case analyzed previously. Additionally, contact resistance occurs between each layer of the substrate but is neglected in this analysis.

Since this orientation is in series, the equivalent resistance in the z direction is a simple sum of each resistance. It is also important to note that T_{out} represents the ambient temperature outside of the iPEBB; this is a different value than the final temperature shown in Figure 7, and T_{out} will likely be smaller than $T_{midsubstrate}$ leading to larger temperature gradient and thus a higher heat flux in the z direction. For now, analysis of equivalent resistance in both cases is enough to determine the broader picture of heat transfer for the substrate. The equation for the total conductive resistance in the z direction is shown below:

$$R_z = R_{cu1} + R_{p1} + R_{cu2} + R_{p2} + R_{cu3}$$
(4)

$$R_z = \frac{1}{A} \left(\frac{L_{cu1}}{K_{cu}} + \frac{L_{p1}}{K_p} + \frac{L_{cu2}}{K_{cu}} + \frac{L_{p2}}{K_p} + \frac{L_{cu3}}{K_{cu}} \right)$$
 (5)

$$R_z = \frac{1}{A} \left(\frac{L_{cu}}{K_{cu}} + \frac{L_p}{K_p} \right) \tag{6}$$

Where L_{cu} represents the total summed thickness of each copper layer within the substrate, and L_p represents the total summed thickness of each polyimide layer.

The equivalent resistance in the z direction is denoted as R_z and can be simplified via the progression shown in the three equations above. The area (A) is the smallest area on the surface of the iPEBB before known heat sources interact in the substrate wall (Figure 9):

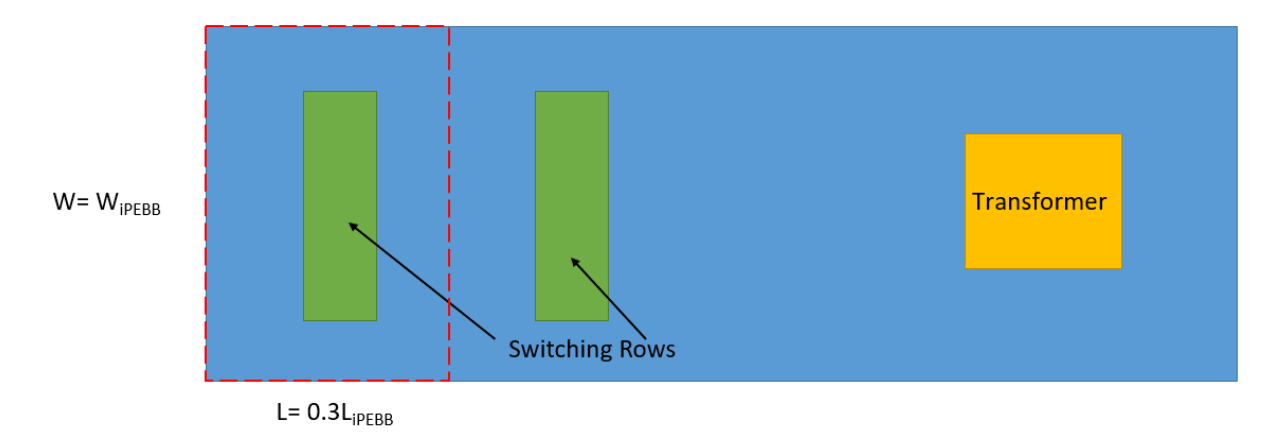


Figure 9: The red square in the image above depicts the area used in the thermal resistance calculation in the z direction. The width is simply the width of the iPEBB, but the length is 0.3 times the length of the iPEBB. This was determined because the maximum length of the resistance area should span from the iPEBB wall to the middle of the two switching rows; this is the smallest length scale that ensures no thermal interactions within the substrate wall from the heat sources.

Thus, the cross-sectional area used in the resistance analysis in the z direction is 0.0495 m². The length terms are essentially the thickness of each layer within the substrate (noted in Figure 5), and each layer of the same material can be summed for an effective length (Eq. 6). Substituting known values:

$$R_{z,substrate} = 0.0087 \frac{K}{W}$$

Comparing the lateral thermal resistance in between the MOSFET rows to the resistance in the z direction, we get the following ratio:

$$\frac{R_{x,Mosfet-Mosfet}}{R_{z,substrate}} = 6.51$$

Similarly, comparing the lateral thermal resistance between the Transformer and the MOSFET row to the resistance in the z direction, we get the following ratio:

$$\frac{R_{x,Mosfet-Transformer}}{R_{z,substrate}} = 11.40$$

Since the thermal resistance in the x direction is larger than the thermal resistance in the z direction through the substrate wall in both cases, we can safely ensure that all the heat transfer in the substrate wall travels strictly in the z direction. This means that the rows of MOSFETS do not interact with each other thermally through conductive modes in the substrate, and similarly, the MOSFETS do not interact with the transformer. This is a critical piece of information because it essentially decouples the transformer and the rows of switches in the heat transfer network, thus, making the model of heat transfer much simpler. It is important to note that although the transformer and the MOSFETS are decoupled conductively, there could still be convective effects due to the ambient air within the iPEBB; these convective heat transfer modes will be analyzed in the subsequent sections that focus on the heat generation sources.

B. Thermal Model of Transformer

The first heat generation source under inspection is the transformer. The first assumption that the current study makes is that we assume that the heat generated within the core of the transformer is evenly distributed throughout the volume of the transformer core (i.e., the top slab, the bottom slab, and the two cylinders connecting the two). By dividing the total heat generation of the core by total volume (0.0161 m³), the heat flux per volume is:

$$q_{core} = \frac{Q_{core}}{V_{core}} = 18.583 \frac{W}{m^3}$$

Since the transformer has two major heat losses, it is important to understand the interaction between the coils and the core of the transformer. Since the transformer system is symmetric across its central horizontal plane and its central vertical plane, it is assumed that the system can be broken

into four identical quadrants with no heat transfer on the borders of each quadrant due to symmetry arguments (Figure 10).

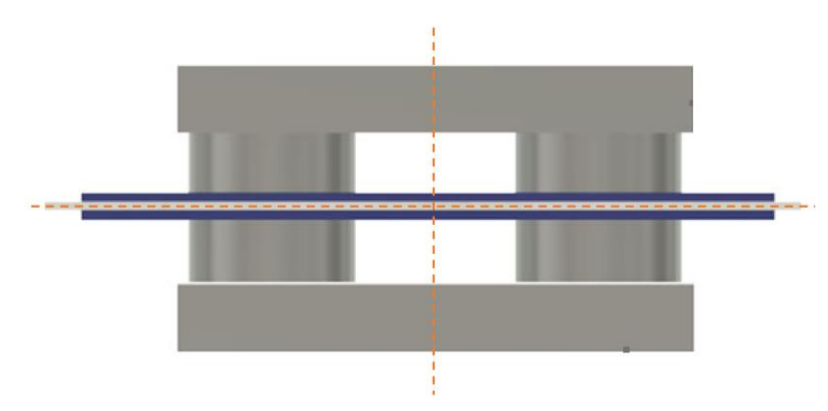


Figure 10: The image above shows the transformer with the planes of symmetry marked in orange dashed lines. Each quadrant in the diagram above has an identical heat transfer network, meaning that the total thermal performance of the transformer is a sum of the four quadrants. This simplifies analysis because the current study can analyze one quadrant and then multiply by a factor of four to determine the result of the entire system. Additionally, since the heat flux leaving a plane of symmetry is identical to the heat flux coming into that plane of symmetry, it can be assumed that total heat flux across the plane of symmetry is zero [8].

Now that the transformer is simplified, we can focus on the thermal effects of the coils in one quadrant. The coils are incredibly important to the transformer system because the coils generate more than double the heat that the core generates. Because these coils are critical for analysis, the next step is to determine how waste heat leaves the coils and interacts with the core. A simplified diagram of the geometric set up is shown below (Figure 11):

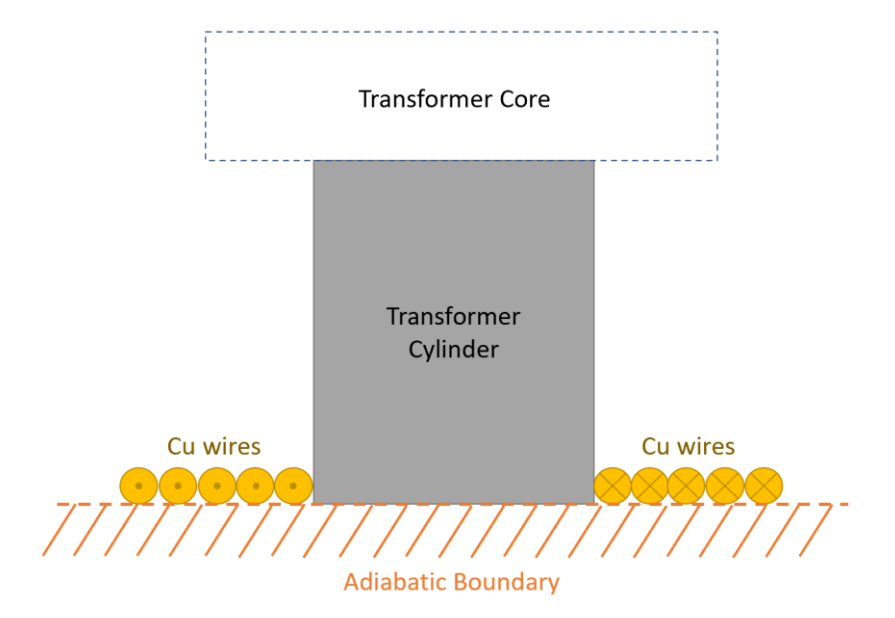


Figure 11: The diagram above depicts the relative geometric relationship between the copper wires and the ferrite cylinder core of the transformer (not drawn to scale). The current version of the transformer has copper wires linearly wrapped around the middle of the transformer cylinder, meaning that only one layer of copper wire is in direct contact with the transformer. Additionally, this image depicts one of the quadrants in the top half of the transformer, meaning that the middle of the transformer is at the bottom of the image shown. This symmetry line is depicted as an adiabatic boundary to the system, so no heat will leave or enter across the dashed line. The top of the transformer is shown as the core at the top of the image.

In the current transformer prototype, the coils are held in the configuration above by a 3D printed plastic casing whose thermal effects are neglected in the current study. Regardless, the copper wires are approximated as a singular solid annulus that generates heat in the middle of the ring (Figure 12).

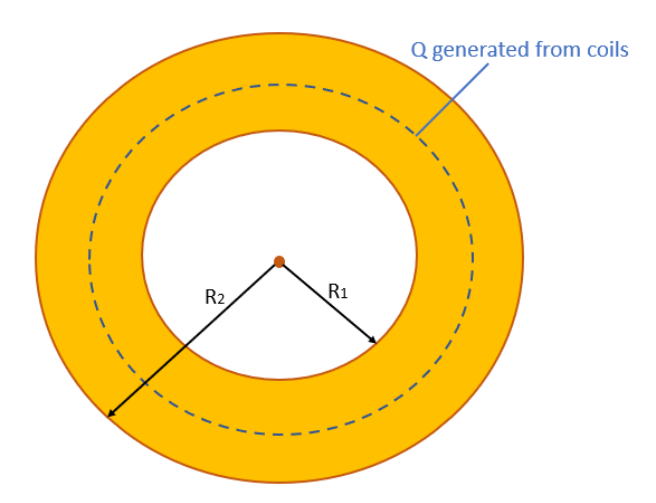


Figure 12: The figure above represents the annulus geometry that the coils are approximated as. It is important to note that the heat generated from this coil is all generated along the central line in the ring (denoted by the blue dashed line). By assuming a singular heat source for the body, the conduction resistance and the convective resistance can easily be calculated.

Using the geometry shown above, we can find the resistance modes and understand where most of the heat flux is located. Using the polar coordinates, the thermal conduction resistance for the disk is shown below (Eq. 7), and the convection resistance is shown in Eq. 8.

$$R_{annulus,cond} = \frac{ln(R_2/R_1)}{2 * \pi * K_{cu} * D} \tag{7}$$

$$R_{annulus,conv} = \frac{1}{h * A_s} \tag{8}$$

Where R_1 is the inner radius of the annulus (5.08cm), R_2 is the outer radius (7.11cm), D is the diameter of a single coil (4.06mm), and h is an assumed average heat transfer coefficient of 10 [W/m^2-K]. Additionally, the surface area (A_s) is a sum of the top and bottom surfaces of the annulus, and the outside surface at R_2 (Eq. 9).

$$A_s = 2(\pi * R_2^2 - \pi * R_1^2) + 2\pi * R_2 * D \tag{9}$$

Plugging in known values we find that the conductive resistance of the coils is:

$$R_{annulus,cond} = 0.0179 \frac{K}{W}$$

The convective resistance of the coils is:

$$R_{annulus,conv} = 5.7597 \frac{K}{W}$$

Since the coils are likely enduring high temperatures, it is critical to analyze potential radiative heat transfer effects to determine if radiation is a major contributor to the spread of heat from the coils. To get an estimate of the total heat flux due to radiation, the Stefan-Boltzmann law is applied to the system:

$$Q_{rad} = \epsilon * \sigma * A * (T_{coil}^2 - T_{core}^2)$$
(10)

Where the emissivity (ϵ) is approximated as roughened copper (0.2), the Stefan-Boltzmann constant (σ) is 5.67*10^-8 [W/(m^2*K^4)], and A is the radiating area and is assumed to be half of the surface area of the annulus. Additionally, the coil temperature was assumed to be the maximum operating temperature of the copper wires (250 degrees Celsius), and the temperature of the core is approximated as 85 degrees Celsius. Plugging known values, we find that the total heat transfer due to radiation is:

$$Q_{coils,rad} = 5.712 \text{ W}$$

Since the convective resistance is over three hundred times greater than the conductive resistance, and the estimated heat transfer from radiation is approximately 1/40 of the total heat generated from the coils, the study assumes that all the heat transfer will go into the cylinder of the core through conductive heat transfer modes only, and the geometry of the transformer problem can simplify into a fin with an applied heat load at the tip (Figure 13).

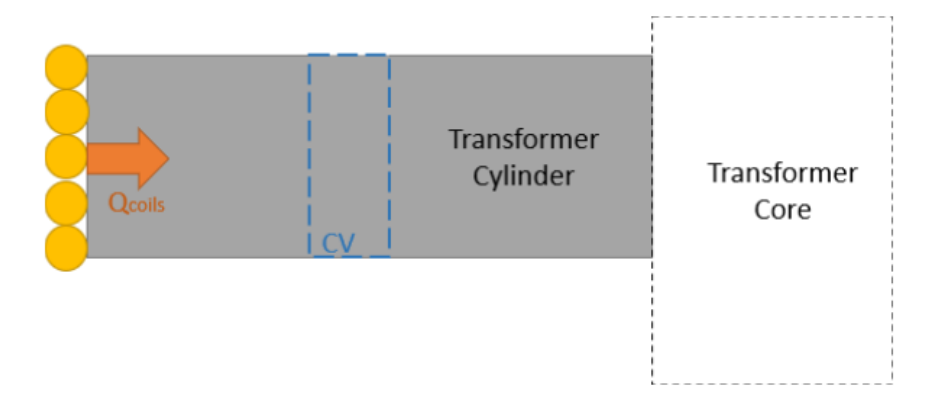


Figure 13: This figure represents the new orientation of the thermal problem with the known heat load from the coils entering the transformer cylinder at the tip. The transformer cylinder can be approximated as a fin with a known applied heat load at the tip. It is important to remember that the transformer cylinder also generates heat evenly throughout the volume.

The heat transfer of this idealized system can be further studied using a control volume within the transformer cylinder (Figure 14) to determine governing equations for the fin behavior.

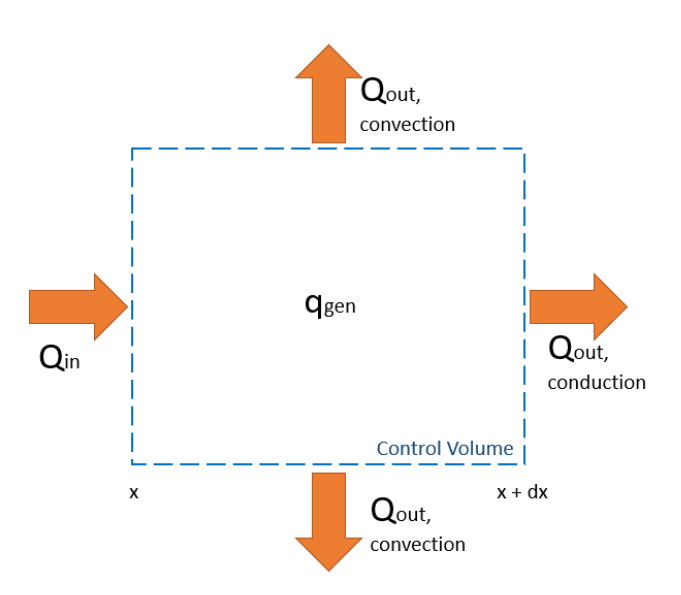


Figure 14: The diagram above represents the control volume denoted in Figure 12. This control volume is helpful to determine the heat fluxes in and out of the body, and it is used to develop the governing equations for the transformer cylinder (shown below). Notably, there are two sources of heat entering the control volume: Q_{in} and q_{gen} . Heat leaves the control volume through convection around the cylinder and conduction in the horizontal direction.

Starting with the first law of thermodynamics (Eq. 11), the system can be solved as follows:

$$\dot{U} = \dot{Q} - \dot{W} \tag{11}$$

$$0 = \dot{Q}_{in} + \dot{q}_{gen}V - \dot{Q}_{out,conv} - \dot{Q}_{out,cond}$$
 (12)

Converting conduction heat fluxes into Fourier's law and clarifying convection:

$$0 = -K\frac{dT}{dx}\Big|_{x=x} *A_c + \dot{q}_{gen}Ac * dx - h * A_s * dT + K\frac{dT}{dx}\Big|_{x=x+dx} *A_c$$
 (13)

where

$$K\frac{dT}{dx}\Big|_{x=x+dx} = K\frac{dT}{dx} + K\frac{dT}{dx}(\frac{d}{dx})dx = K\frac{dT}{dx}\Big|_{x=x} + K\frac{d^2T}{dx^2} * dx \tag{14}$$

Plugging Eq. 14 into Eq. 13, the equation simplifies to:

$$0 = +\dot{q}_{gen}Ac * dx - h * A_s * dT + A_c \left(K\frac{d^2T}{dx^2}dx\right)$$

$$\tag{15}$$

Inserting terms for A_c and A_s :

$$h(2\pi R dx)dT = \pi R^2 dx \left(\dot{q}_{gen} + K \frac{d^2 T}{dx^2}\right)$$
 (16)

Simplifying:

$$2h(T(x) - T_{\infty}) = R\left(\dot{q}_{gen} + K\frac{d^2T}{dx^2}\right) \tag{17}$$

Let:

$$\theta(x) = T(x) - T_{\infty} \tag{18}$$

Where T_{∞} = 20 degrees Celsius (assumed to be room temperature)

After plugging in Eq. 18 to Eq. 17 and rearranging terms, the final differential equation is shown below (Eq. 19):

$$-\dot{q}_{gen} = K \frac{d^2\theta}{dx^2} - \frac{2h}{R}\theta\tag{19}$$

Solving the differential equation gives us a temperature distribution along the cylinder:

$$\theta(x) = C_1 e^{\sqrt{\frac{2h}{KR}}x} + C_2 e^{-\sqrt{\frac{2h}{KR}}x} + \frac{\dot{q}_{gen}R}{2h}$$
 (20)

Where C_1 and C_2 are constants that can be found by imposing known boundary conditions:

1) At
$$x_{\text{fin}} = 0$$
, $T_{fin(x_{fin}=0)} = 240^{\circ} C$

2) At
$$x_{\text{fin}} = 0$$
,
$$-K_{iron} A_{fin} \frac{dT}{dx} \Big|_{x_{fin} = 0} = Q_{coils}$$

The first boundary condition is imposed as the maximum temperature (the Curie temperature) of the transformer. Since we know that the system behaves like a fin, the highest temperature would have to be at the tip closest to the large heat source coming from the coils. By imposing a temperature boundary condition, the system of equations will display a temperature profile of the worst-case scenario of the transformer overheating.

The second boundary condition regarding the heat flux at x_{fin} = 0 is known because all the heat entering the system at the tip is due to the waste heat from the coils. Through the first law of thermodynamics, the heat flux into the system is equal to the heat flux out of the system in steady state as shown in boundary condition 2.

After finding constants from known boundary conditions, the temperature profile along the fin is known (Eq. 21):

$$C_1 = -50.34$$

$$C_2 = 137.89$$

$$T_{fin}(x) = -50.34e^{\sqrt{\frac{2h}{KR}}x} + 137.89e^{-\sqrt{\frac{2h}{KR}}x} + \frac{\dot{q}_{gen}R}{2h} + T_{\infty}$$
 (21)

Now that we know the temperature profile of the transformer fin, we can now solve for the temperature profile of the rectangular core using similar analytical methods. The first step is to check the Biot condition in the core to determine the relative effect of convection. The geometry of the transformer core is shown below (Figure 15).

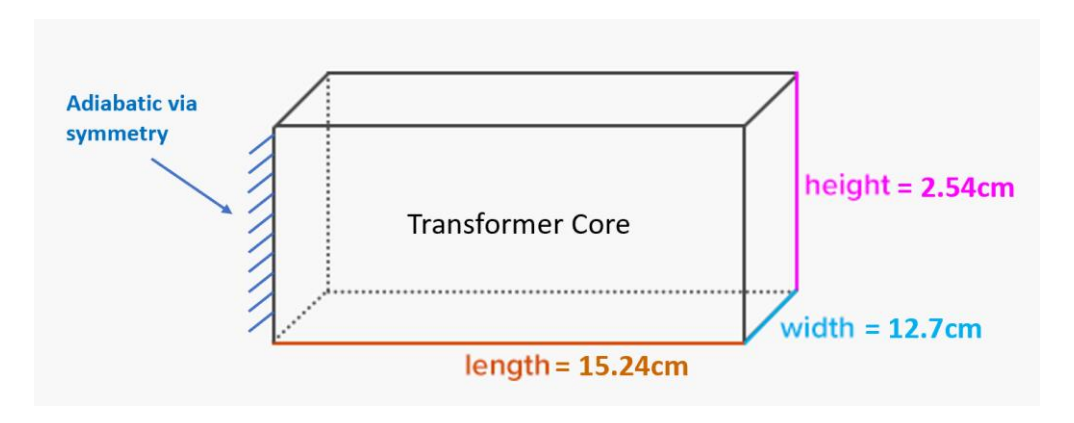


Figure 15: The diagram above depicts the geometry of the one fourth of the transformer core. It is important to note that the core is adiabatic on two sides due to symmetry (the left side and the rear side shown in the image). Therefore, the surface area for convection is the front and right sides of the rectangular prism. Additionally, the cross-sectional area for conduction is the area of the top side of the prism.

Using the Biot Equation, we find the ratio of conductive resistance to convective resistance:

$$Biot = \frac{R_{cond}}{R_{conv}} = \frac{hl}{k} \tag{22}$$

Solving the Conduction and Convection resistance of the core (See Appendix A for detail), we find that the Biot number is very small:

$$Bi_{core} = 6.9 * 10^{-4}$$

Since the Biot number is much less than zero, it can be assumed that the convective resistance is much larger than the conductive resistance, and thus all heat transfers through conduction in the core. Now the problem can be solved in a similar manner to the cylinder using the first law of thermodynamics.

In this analysis, the current study intends to add a superconductor cut in the thermal model shown in Figure 16:

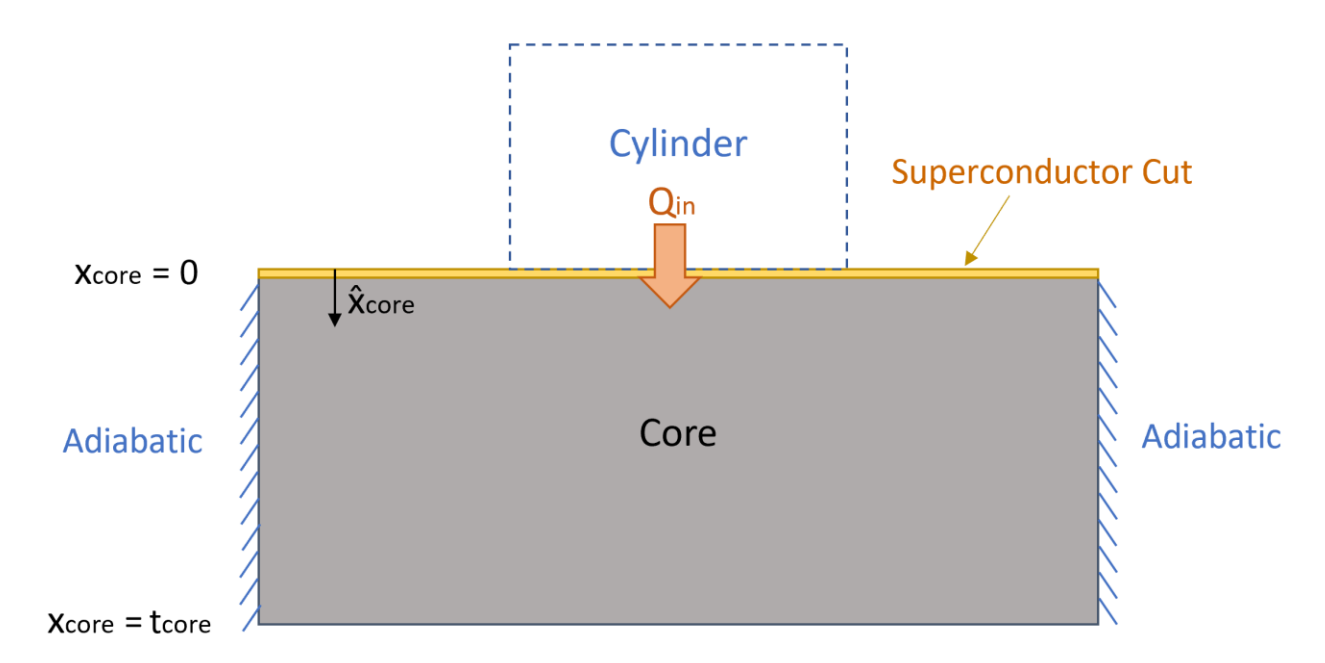


Figure 16: This diagram shows the thermal assumptions utilized in the analysis of the transformer core. At xcore = 0, the model inserts an infinitely thin superconductor cut into the core. This allows infinite heat spreading across the surface, and the temperature along the surface of xcore= 0 is assumed to be constant. This is an effective first order model because it reduces the complexity to a one-dimensional problem. Additionally, the core has adiabatic walls shown in the diagram in accordance with the Biot calculation proving no lateral heat transfer.

The superconductor cut is valid for this model because the heat transfer due to convection on the top surface is negligible. In addition, the ratio of the cross-sectional area of the cylinder to the cross-sectional area of the core is 0.42 meaning that almost half of the cross-sectional area of the core is in contact with the cylinder. This assumption induces a small error into the calculation and should be addressed in future iterations of the thermal model.

Using the assumptions explained above to form the framework for this calculation, we can use the first law of thermodynamics to derive the temperature gradient through the core similar to the analysis done with the cylindrical fin in the previous section.

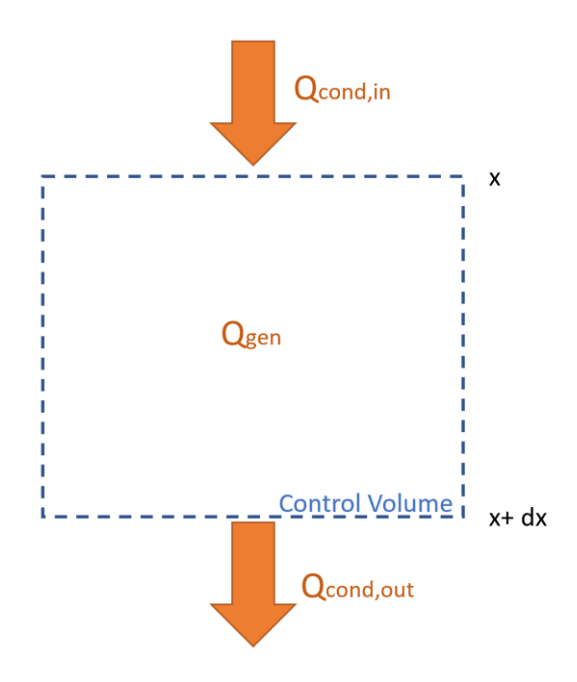


Figure 17: This figure represents a control volume within the transformer core. It is important to note that there are no convection heat transfer modes in this model, and the first law of thermodynamics only includes conduction and heat generation by the transformer core.

Using the control volume above, we can find a differential equation for the transformer core through the first law of thermodynamics (Eq. 23). Using the same analytical methods as shown in the cylindrical fin of the transformer, the present study can derive a temperature profile along the thickness of the transformer core (Eq 25). Further detail is displayed in appendix B.

$$-K\frac{dT}{dx}\Big|_{x_{core}=x}A_{core}+\dot{q}_{gen}A_{core}dx+K\frac{dT}{dx}\Big|_{x_{core}=x+dx}A_{core}=0 \tag{23}$$

Simplifying with algebra and partial derivatives:

$$\left(\frac{-q_{core}}{K_{iron}}x + D_1\right)dx^2 = d^2T \tag{24}$$

Integrating twice:

$$\frac{-q_{core}}{2K_{iron}}x^2 + D_1x + D_2 = T(x_{core})$$
 (25)

Where D_1 and D_2 are constants that can be found by imposing the boundary conditions shown below:

1) At
$$x_{core} = 0$$
 $T(x_{core} = 0) = T(x_{cylinder} = L_{cylinder})$

2) At
$$x_{core}=0$$

$$-K_{iron}\frac{dT}{dx}A_{cylinder}\Big|_{x_{cylinder}=L_{fin}} = -K_{iron}A_{core}\frac{dT}{dx}\Big|_{x_{core}=0}$$

The first boundary condition asserts that the temperature at the inner surface of the core is the same as the temperature at the base of the cylindrical fin (the part farthest from the coils). This is reasonable because the temperature at the interphase junction between two materials in contact is the same for both materials. This assertion is further enforced by the superconductor cut assumption, meaning that the entire core at $x_{core} = 0$ is assumed to be isothermal.

The second boundary condition is the heat flux boundary conditions. Since the Biot calculation established that conduction is the only heat transfer mode in the core, we know that the entire heat flux into the core must be equal to the heat flux out of the cylinder at its base. Therefore, using Fourier's law, we know that the heat flux due to conduction at the interphase of the core ($x_{core} = 0$) is equal to the heat flux due to conduction out of the cylinder at $x_{cylinder} = L_{cylinder}$.

After finding constants from known boundary conditions, the temperature profile along the fin is known (Eq. 26):

$$D_1 = -66.49$$

 $D_2 = 231.868$

$$\frac{-q_{core}}{2K_{iron}}x^2 - 66.49x + 231.868 = T(x_{core})$$
(26)

The final step in the analysis of the heat transfer is to find the thermal gradient through the substrate wall of the iPEBB. This analysis is very similar to the previous work shown in the thermal analysis of the core, except it is less complex because there is no heat generation in the substrate. This means that the temperature gradient derived from the first law of thermodynamics only has conduction modes (See Appendix C for more detail). Additionally, this temperature gradient is confined to the region directly in the path of the transformer, so the cross-sectional area is limited to the cross-sectional area of the transformer core. Lateral heat spreading effects for the transformer are neglected because the transformer has a very large conductive cross-sectional area compared to the thickness of the substrate and heat spreading effects would only marginally increase the total area. Thus, the increase in area due to spreading is negligible compared to the original cross-sectional area.

First law of thermodynamics in the substrate:

$$-K\frac{dT}{dx}\Big|_{x_{substrate}=x} A_{core} + K\frac{dT}{dx}\Big|_{x_{substrate}=x+dx} A_{core} = 0$$
 (27)

Simplifying through algebra and partial derivative identities:

$$\frac{d^2T}{dx^2} = 0\tag{29}$$

Integrating twice to find the temperature distribution in the substrate:

$$T(x_{substrate}) = e_1 x + e_2 (30)$$

The boundary conditions are very similar to the core:

1) At
$$x_{substrate} = 0$$
 $T(x_{substrate} = 0) = T(x_{core} = t_{core})$

2) At $x_{substrate} = 0$

$$-K_{substrate} \frac{dT}{dx} \Big|_{x_{substrate}=0} = -K_{iron} \frac{dT}{dx} \Big|_{x_{core}=t_{core}}$$

The reasoning behind the boundary conditions for the substrate is the same as previously described for the transformer core. First, the temperature must be the same at the contact point between the transformer core and the inside surface of the substrate. Secondly, since the only mode of heat transfer is conduction, the flux of heat transfer that conducts out of the core at the substrate interface must be equal to the heat flux into the substrate at $x_{substrate} = 0$. This is shown through Fourier's law in the second boundary condition.

Notably, the substrate consists of multiple layers of material. For the purposes of this analysis, the conductive performance of the substrate can be estimated using an average coefficient of thermal conductivity ($K_{substrate}$). This can be found by equating the total conductive resistance of the substrate to the resistance of the copper and polyimide layers (Eq. 31). Then K_{eff} is found

through algebraic analysis of the equivalent resistances. It is important to note that contact resistance is neglected in this analysis because we assume good manufacturing processes that ensure sufficiently firm contact between the layers so as to make the contact resistance negligible.

$$R_{substrate} = R_{cu} + R_{polyimide}$$
(31)

$$\frac{t_{substrate}}{K_{eff}A_{core}} = \frac{t_{cu}}{K_{cu}A_{core}} + \frac{t_p}{K_pA_{core}}$$
(32)

Where t_{cu} is the total thickness of copper in the substrate (5.8mm), and t_p is the total thickness of polyimide (0.05mm).

$$\frac{t_{substrate}}{K_{eff}} = \frac{K_{cu}t_p + K_pt_{cu}}{K_{cu}K_p} \tag{33}$$

$$K_{eff} = \frac{K_{cu}K_{p}t_{substrate}}{K_{cu}t_{p} + K_{p}t_{cu}}$$
(34)

Plugging in known properties:

$$K_{eff} = 13.565 \frac{K}{W}$$

Since K_{eff} is defined as the average coefficient of conductivity in the substrate, the current study can now redefine the substrate as a single material with a conductivity of K_{eff} . This is effective for temperature gradient analysis because it incorporates the thermal properties of the entire substrate without having to individually analyze each layer.

Solving boundary condition equations reveals the temperature profile through the substrate (Eq. 35):

$$e_1 = -408.285$$

 $e_2 = 230.09$

$$T(x_{substrate}) = -408.285x + 230.09 (35)$$

Now that we have the temperature profile through the substrate, we can plug in the thickness of the iPEBB substrate wall to determine what the temperature of the outside wall of the iPEBB is at the curie temperature:

$$T(x_{substrate} = t_{substrate}) = 227.72 \, ^{\circ}C$$

Additionally, the heat flux through the outer substrate wall can be determined by a first law analysis of the substrate at the outside thickness (Eq. 36):

$$-K_{eff}A_{core}\frac{dT}{dx}\Big|_{x_{out}=t_{out}} = Q_{out}$$
(36)

Plugging in known values:

$$Q_{out} = 214.397 \text{ W}$$

This is significant because to keep the transformer under its Curie temperature, the outside wall of the iPEBB must be below 223.5 degrees Celsius. This means that the method of cooling for the transformer system must be capable of meeting this temperature requirement. Furthermore, an adequate cooling system can be designed around this temperature constraint by simply creating a thermal circuit with a known maximum temperature and a known heat flux out. It is important to note that the total heat flux from the transformer out of one side of the iPEBB is two times the heat Qout because there are two symmetric heat sources that heat up one wall of the iPEBB.

$$Q_{TransformerSubstrate} = 428.794 \text{ W}$$

Additionally, the temperature profile from the tip of the cylinder to the outer surface of the substrate is depicted in Figure 18:

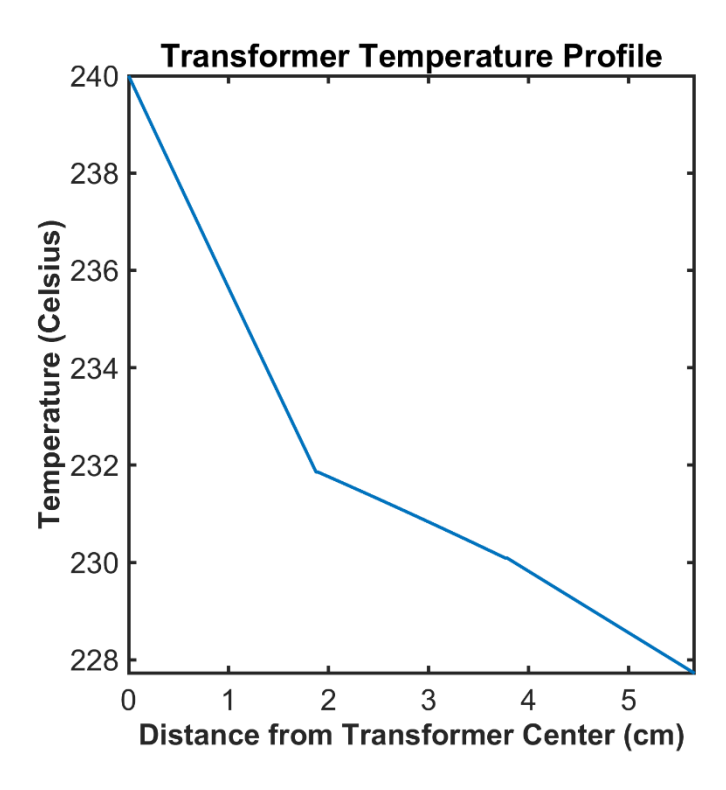


Figure 18: The graph above displays the temperature within the Transformer and Substrate from the center of the transformer (x=0 cm) to the outer wall of the iPEBB (x=5.66 cm). This graph quickly visualizes the effects of the three different parts of the transformer system which are depicted by having different slopes on the graph.

This graph is reasonable because the maximum temperature is at the tip of the cylinder where the coils generate heat, and the different slopes represent different conditions within each piece of the system such as heat flux into the ambient air by the cylinder, different cross-sectional areas, and different coefficients of conductivity.

C. Thermal Model of MOSFETs

The second thermal source needing to be modeled consists of the four MOSFET row systems (described in section 3 of the Background). This source is arguably the most challenging aspect of the thermal cooling system because the total switching system accounts for 4752W in total losses throughout the switching system, with each MOSFET producing 49.5W of waste heat. Notably, this is more than four times the total losses in the transformer system (1100W). Due to this high heat flux, it is likely necessary that the switching system will need a more robust cooling method than the previous transformer system.

The first step is to check the Biot number of an individual MOSFET to determine the relative effect of convection to conduction. This is done as before by taking the ratio of conductive resistance to convective resistance. Additionally, the heat source is assumed to be generated at the centroid of the MOSFET, so the length scale of conduction is half the thickness of the MOSFET.

$$R_{Cond.Mosfet} = \frac{t_{mos}}{2K_{mos}s_{mos}^2} \tag{37}$$

$$R_{Conv.Mosfet} = \frac{1}{h_{mos}(4t_{mos}s_{mos} + s_{mos}^2)}$$
(38)

Where h_{mos} = 5 [W/m^2-K] and represents an average heat transfer coefficient for natural convection on a flat plate.

$$Biot_{Mosfet} = \frac{R_{Cond.Mosfet}}{R_{Conv.Mosfet}} = 4.5 * 10^{-5}$$
(39)

Since the Biot number of the MOSFET is much less than one, heat transfer through convective modes can be neglected, and the thermal problem can simplify to one dimension through the substrate.

Since the switches are placed in rows with an edge distance of 1cm between switches, it is worth doing further analysis to determine heat spreading effects to estimate the thermal interactions between switches.

For the analysis of heat spreading, various academic literature provides some reasonable correlations that were measured from experimental findings. Notably, R. Simmons details in [9] methods that approximate a single square heat source as a circle with equivalent area and uses non-dimensional geometric variables and quantifiable heat sinks to determine the spreading resistance. Additionally, literature provides examples of approximating a column of power transistor heat sources. This method asserts that the closeness of individual heat sources can be approximated as a single, large rectangular heat source. Similarly, this method has non-dimensional length scales and uses graphical correlations to determine the spreading resistance with a known heatsink to cool the system [10]. Both methods have merit, but they are not accurate tools for the current study because of various aspects of uncertainty.

Firstly, correlations found in literature assume heat spreading is through a single plate. This is problematic for the current study because the substrate wall has multiple layers of different materials, and the lateral heat spreading due to different resistances in materials is not reflected in previous literature correlations. Secondly, the literature correlations place heat sources on heat spreading plates with known dimensions. In the iPEBB, the dimensions of the effective heat spreading plate are uncertain because the switches are placed on a very large substrate wall that also interacts with other heat sources. This means that the area of an effective heat spreading plate was arbitrarily determined using symmetry assumptions between heat sources (i.e., the boundary of an effective plate is midway between two MOSFET rows). Lastly, previous literature assumes a known, quantifiable cooling system that is actively used in analysis, but the current study does not have a known cooling system within the model. To complete the literature correlations, a heat sink would have to be estimated. Any use of the literature correlation techniques would be riddled with uncertainty and was deemed unfit for the current application.

Another common theory that models heat spreading is to add a heat spreading angle from the heat source so that the area affected by conduction increases through the thickness of the wall. The most common method is to add a 45-degree heat spreading angle, but this method is known to have an error as large as 30% through a uniform plate [11]. This error will likely be compounded by the current application because the substrate wall consists of layers of copper and polyimide. Since polyimide has a much smaller thermal conductivity than copper, the heat will likely conduct laterally through the copper and only partially flow vertically through the polyimide layer (Figure 19).

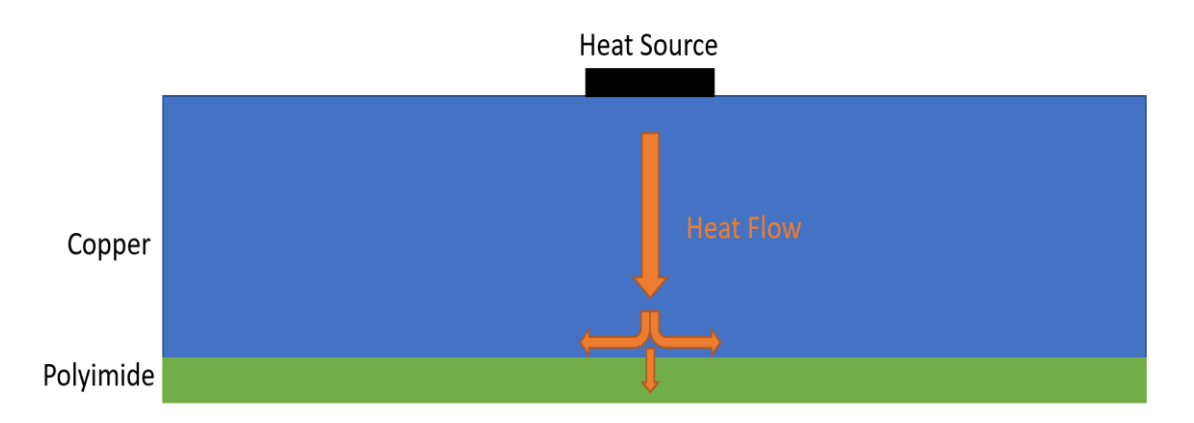


Figure 19: The image above is a simple representation of how the different conductive resistances will impact heat flow through the substrate wall. Polyimide has a much higher resistance than Copper, and heat will spread laterally at the interface between copper and polyimide as shown. Since the substrate has two layers of polyimide, this heat spreading behavior will occur twice through the substrate wall.

It is important to note that although there is lateral heat flow, it is not extensive enough that the heat sources interact (as proven in section III, A). Heat spreading is extremely difficult to quantify, and it is possible to do vigorous two-dimensional analysis to approximate the full effect, but for the purpose of this study we will continue with an effective heat spreading angle. Since it is established that the 45-degree heat spreading angle is relatively inaccurate and likely not fit for this application, the current study intends to derive a rough estimate of the heat spreading angle through experimentation as explained below.

a. Heat Spreading Experimentation

i. Experimental Design

This experiment was designed to estimate the amount of heat spreading via lateral conduction at the interface of a thick conductive material and a thin insulative material. A heat source was placed on one side of the substrate and the temperature of both sides of the substrate was measured after the system reached its steady state response (Figure 20).

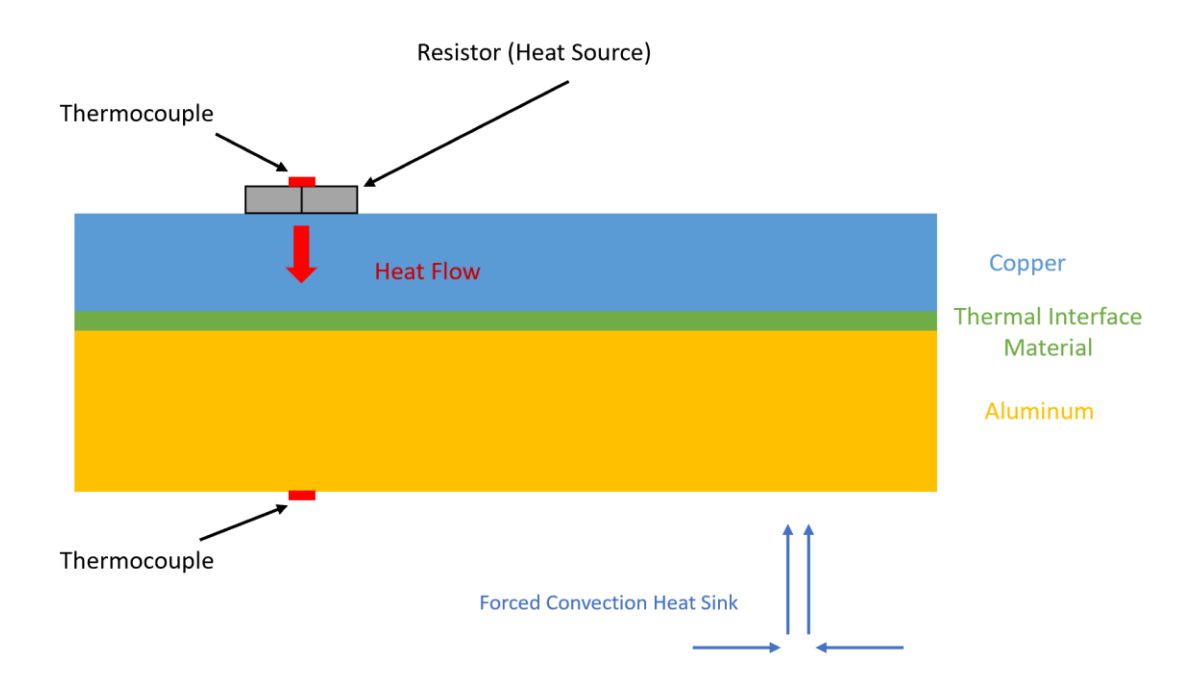


Figure 20: This diagram above is a simple rendering of the experimental set up designed to calculate an effective spreading angle. It is important to note that the substrate consists of three materials: Copper, a thermal interface material (Si-98), and Aluminum. Additionally, the heat source is placed on the bottom of the substrate with all the heat produced conducting through the wall of the substrate.

As noted in Figure 19, two thermocouples are placed on opposite sides of the system; one thermocouple is directly attached to the bottom of the heat source, and the other is placed directly to the outer layer of aluminum. These thermocouples directly measure the temperature gradient across the system and were chosen instead of an infrared camera because thermocouples have greater precision. Forced air convection was utilized to cool the top layer of substrate to provide a clear temperature gradient within the thickness of the substrate. This is essential because this acts as a heat sink and reduces the problem to one-dimensional heat transfer. If the fan was not incorporated in this experiment results would not be valid because natural convection would be the dominant cooling method that acts on every outer surface of the substrate, and the heat transfer problem would no longer be a one-dimensional problem. Furthermore, this experiment is designed to perform one-dimensional heat transfer because the MOSFET system in the iPEBB behaves in one dimension (as demonstrated in section III, A).

The geometric length scales and thermal properties of each material in the experiment are defined in the following table:

Table 2

Material	Length (cm)	Width (cm)	Thickness (cm)	Thermal
				Conductivity
				(W/m-K)
Resistor	7.62	2.54	1.22	N/A
Copper	15.24	15.24	0.475	398
Si-98	15.24	15.24	0.015	0.9
Thermal				
Interface				
Material				
Aluminum	15.24	15.24	1.27	237

Although this experiment does not exactly model the iPEBB substrate wall, it still provides valuable insights into how heat spreads in a multilayered substrate. In this experiment, the Si-98 thermal interface material and the copper layer adequately represent the thermal spreading of the first copper/polyimide interface on the inner side of the iPEBB substrate wall. This is because this experiment closely resembles the ratio of thermal resistances at the interface layer in the iPEBB.

The ratio of conductive resistance of the inside copper layer and polyimide is shown below:

$$\frac{R_{Cu,substrate}}{R_{poly,substrate}} = 0.036$$

The ratio of conductive resistance of the experimental copper layer and Si-98 is shown below:

$$\frac{R_{Cu,experiment}}{R_{Si98,experiment}} = 0.071$$

The conductive resistances of each layer were determined through Fourier's law of thermal conduction.

The ratio of conductive resistances reflects the relative ease of heat to flow from one layer to another. For example, if the resistance ratio was equal to one, then the two layers would have the exact same thermal resistances, and heat would continue to flow unidirectionally through the substrate wall. However, a very low resistance ratio indicates that one substrate layer is much more thermally resistant than the other, and heat spreading will occur because the lateral resistance of the top layer is much smaller than the vertical resistance through the second layer. The current experiment mimics this effect within the iPEBB because the thermal resistance ratio between layers is very similar to what occurs in the real system since the ratios shown above are roughly equivalent (and certainly within the same order of magnitude).

ii. Experiment Data Collection

The experiment has a simple procedure by adding 22.5 Watts of power to the resistors and allowing the experiment to continue until the two thermocouples reached steady state. At the end of the experiment, the bottom thermocouple had a constant temperature of 48 degrees Celsius, and the top thermocouple displayed a constant temperature of 47 degrees Celsius. Since the temperature gradient is known, and the heat output is known, the total thermal resistance through the experimental substrate can be found using a simple first law energy balance and reduces to Eq 40:

$$R_{experiment} = \frac{T_{bottom} - T_{top}}{Q_{resistors}} = 0.044 \frac{K}{W}$$
 (40)

iii. Calculating Experimental Heat Spreading Angle

Since the measured thermal resistance through the experimental substrate is 0.0444 [K/W], we must determine a thermal resistance via analytical methods that is equal to the experimental resistance to have a reliable analytical model. This can be achieved by back solving for an effective heat spreading angle that increases the area of conduction. It is known that the total resistance of the experimental substrate is the sum of the conductive resistance of each layer (Eq. 41):

$$R_{experiment} = R_{cu} + R_{im} + R_{al}$$

$$\tag{41}$$

$$R_{experiment} = \frac{t_{cu}}{K_{cu}A_{cu}} + \frac{t_{im}}{K_{im}A_{im}} + \frac{t_{al}}{K_{al}A_{al}}$$
(42)

Since the heat spreading angle increases the cross-sectional area, the area for each material represented in Eq. 42 is different. Since the area of conduction increases along the thickness of each material, the average area of the material is needed for analysis that can be found by

multiplying the average length by the average width. A visual depiction of the heat spreading angle and the change in increased side length is shown below (Figure 21).

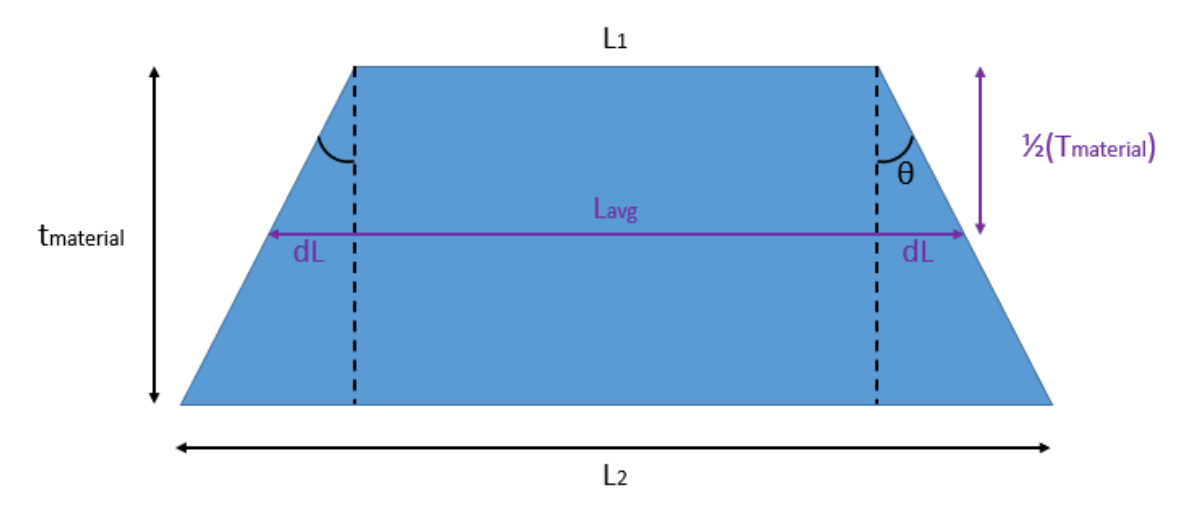


Figure 21: The diagram above represents a heat spreading angle through the thickness of a conductive material as heat flows downwards. Note that the length of the bottom of the trapezoid depends on the original length of the heat source and the heat spreading angle. Additionally, the average length within the substrate thickness occurs at one half of the thickness of the material (shown in purple). Note that dL represents the additional increase in length due to the heat spreading angle.

The average length due to heat spreading within a substance can be calculated as shown in Eq. 43:

$$L_{avg} = L_1 + 2dL \tag{43}$$

Where:

$$dL = \left(\frac{t}{2}\right) \tan(\theta) \tag{44}$$

Plugging (44) into (43):

$$L_{avg} = L_1 + t_{material} tan(\theta) \tag{45}$$

Similarly:

$$W_{avg} = W_1 + t_{material} tan(\theta) \tag{46}$$

Where L_1 and W_1 represent the length and width of the conductive area at the first edge of the substrate layer (the top side of the trapezoid shown in Figure 21 and the bottom side of the material layer in Figure 20).

Using Eq. 45 and 46, the conductive areas of each material in the substrate are as follows:

$$A_{cu} = (L_{resistor} + t_{cu}tan\theta)(W_{resistor} + t_{cu}tan\theta)$$
(47)

$$A_{im} = \left(L_{resistor} + (2t_{cu} + t_{im})tan\theta\right)\left(W_{resistor} + (2t_{cu} + t_{im})tan\theta\right) \tag{48}$$

$$A_{al} = \left(L_{resistor} + (2t_{cu} + 2t_{im} + t_{al})tan\theta\right)\left(W_{resistor} + (2t_{cu} + 2t_{im} + t_{al})tan\theta\right)$$
(49)

Where $t_{material}$ from Eq. 45 and 46 is reflected as the distance from the edge of the experimental substrate where the heat load is applied to the farthest edge of the material under inspection. This is reflected in the term multiplied by $tan\theta$ in Eq. 47, 48, 49.

The spreading angle (θ) is determined by inserting equations 47, 48, 49 into Eq. 42:

$$\theta_{spread} = 67.3^{\circ}$$

iv. Discussion

After through experimentation and analysis, the heat spreading angle was determined to be 67.3 degrees, thus for a substrate that has two layers with vastly different thermal resistances, a heat spreading angle of 67.3 is sufficient in encapsulating the two-dimensional heat spreading effects. This is significant because it is much larger than the 45-degree heat spreading angle used in common practice, and it proves that there is significant heat spreading in a multilayered conductive system where the highly resistive substance essentially slows flow vertically through the substrate and forces heat to travel laterally through the less resistive material.

Although the resulting heat spreading angle makes sense intuitively, there are a couple factors introducing uncertainty into the experiment. First, the temperature of the heat source was measured at the top of the resistor. If the experiment could measure the temperature at the interface of the resistor and copper layer, the temperature gradient would be more precise; however, the

present study was unable to measure in this location because it is impossible to place our thermocouple or other temperature measuring equipment in that space. In this study, the contact resistance of the resistors is neglected, and it is assumed that the heat source is directly applied to the surface of the experimental substrate. Secondly, contact resistance in the experiment was neglected in analysis. Lastly, the ratio of conductive resistances in the experiment is about twice as large as the ratio of conductive resistance in copper/polyimide interface layer in the iPEBB. To improve the accuracy of the results, the ratio of conductive resistance can be decreased by running the experiment with a thinner copper plate (thus decreasing the conductive resistance of the copper).

This experiment provides insight into heat spreading in a multilayered substrate, and the spreading angle calculated will be used in further analysis of conduction through the iPEBB substrate; however, the heat spreading angle that is representative of the iPEBB substrate is likely larger than the angle calculated through experimentation. This is because the iPEBB substrate wall has three layers of copper and two layers of polyimide, so heat spreading will likely occur in the two interfaces when heat flows from the copper to the polyimide whereas the experiment only calculated heat spreading in one critical interface. The only way to determine a true spreading angle for the substrate is to perform a similar experiment but through the iPEBB substrate wall.

b. iPEBB MOSFET Heat Spreading Analysis

Now that an acceptable spreading angle is known, more analysis is needed to determine if the switching system should be modeled as individual MOSFETs that generate heat or if it would be better to estimate the entire row into a singular heat source. If individual MOSFETs interact thermally with neighboring MOSFETs in the substrate, it would be better to approximate the system as a single rectangular heat source. Further analysis using the heat spreading angle is needed to locate where the spreading area of MOSFETs intersect within the iPEBB wall (Figure 22).

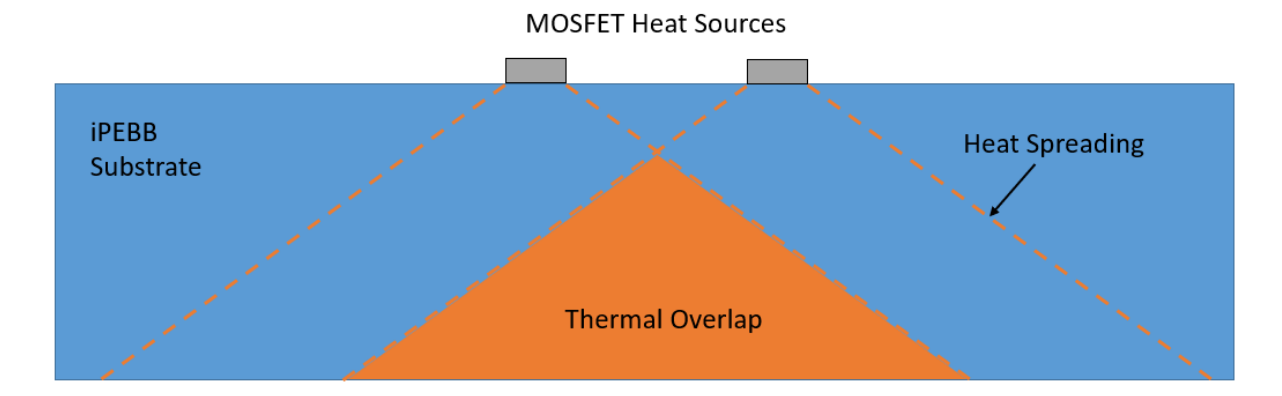


Figure 22: The image above demonstrates the issue of thermal overlap within the iPEBB wall (not drawn to scale). If there is significant thermal overlap between two heat sources, the appropriate model would be to approximate the switches as one large rectangular heat source that covers the entire surface area within the MOSFET rows. If there is minimal thermal overlap, the better model would be to calculate the resistance of individual MOSFETs and sum them in a parallel resistance network.

The MOSFETs in a row are placed 1 cm apart from edge to edge, so the thermal overlap would occur at half this separation distance, or 0.5 cm from the edge of a MOSFET. Using trigonometry and plugging in the thermal spreading angle, we can find the depth of into the wall where the intersection point occurs (Eq. 50):

$$t_{intersect} = \frac{x_{overlap}}{tan\theta} = 2.1 \text{ mm}$$
 (50)

Since the thermal spreading area intersects in the substrate 2.1 mm from the surface with the heat source, it can be assumed that there is significant thermal spreading and prolific thermal interactions between the heat flux of each MOSFET within the iPEBB substrate. Furthermore, since the total thickness of the substrate is 5.8 mm, the intersection point is just over a third of the total thickness, and most of the substrate will be in the thermal overlap space shown in Figure 22. The best model to represent the thermal resistance of the system would be to model the row of MOSFETS as one singular heat source. The surface area of the single rectangular row is equivalent to the outside distance from MOSFETS along the length times the outside distance of the width:

$$L_{row} = 0.24 \ m$$

$$W_{row} = 0.03 \ m$$

$$A_{row} = 0.072 \ m^2$$

Applying Eq. 45 and 46, we can solve for the effective area of each layer of the substrate by adding the additional area growth due to the heat spreading angle. For this application $t_{material}$ noted in Eq. 45 and 46 represents the distance from the surface of the heat source to the bottom edge of the material under inspection.

The total conductive resistance through the substrate wall is the sum of the resistance of each layer within the substrate:

$$R_{substrate} = R_{Cu1} + R_{p1} + R_{Cu2} + R_{p2} + R_{Cu3}$$
(51)

$$R_{substrate} = \frac{t_{Cu1}}{K_{Cu}A_{Cu1}} + \frac{t_p}{K_pA_{p1}} + \frac{t_{Cu2}}{K_{Cu}A_{Cu2}} + \frac{t_p}{K_pA_{p2}} + \frac{t_{Cu3}}{K_{Cu}A_{Cu3}}$$
(52)

Using the heat spreading theory stated in Eq. 45 and 46 we can find the average area of each element within the substrate:

$$A_{Cu1} = (L_{row} + t_{Cu1}tan\theta)(W_{row} + t_{Cu1}tan\theta)$$
(53)

$$A_{p1} = (L_{row} + (2t_{Cu1} + t_p)tan\theta)(W_{row} + (2t_{Cu1} + t_p)tan\theta)$$
(54)

$$A_{Cu2} = (L_{row} + (2t_{Cu1} + 2t_{tp} + t_{Cu2})tan\theta)(W_{row} + (2t_{Cu1} + 2p + t_{Cu2})tan\theta)$$
(55)

$$A_{p2} = \left(L_{row} + (2t_{Cu1} + 3t_p + 2t_{Cu2})tan\theta\right)\left(W_{row} + (2t_{Cu1} + 3t_p + 2t_{Cu2})tan\theta\right)$$
(56)

$$A_{Cu3} = (L_{row} + (2t_{Cu1} + 4t_p + 2t_{Cu2} + t_{Cu3})tan\theta)(W_{row} + (2t_{Cu1} + 4t_p + 2t_{Cu2} + t_{Cu3})tan\theta)$$
(57)

After plugging the area equations into Eq. 52, the total equivalent resistance of the substrate is:

$$R_{substrate} = 0.0344 \frac{K}{W}$$

Now that the thermal resistance of the system is known, the temperature of the outside of the iPEBB needed to keep the MOSFET system under the critical temperature of 150 degrees Celsius is found using a simple thermal circuit that reduces to Equation 58:

$$T_{out,mosfet} = Tin, mosfet - Q_{row}R_{substrate}$$
 (58)

where Q_{row} is one fourth of the total heat flux due to the switching system in the iPEBB since there are four rows of MOSFETs

Solving with known values:

$$T_{out.mosfet} = 109.16$$
 °C

This is a very reasonable estimate for a temperature on the outside of the iPEBB wall for a MOSFET row system because the temperature gradient from the MOSFET to the outer wall is only a 40-degree Celsius difference. T_{out,mosfet} represents the maximum temperature on the outside substrate wall in order to keep the switching system under its operation temperature. Additionally, the entire surface area affected by the spreading angle needs to be cooled:

$$A_{out,mosfet} = 0.0155$$
m²

This result is helpful for future work into designing a cooling system because there is now a quantifiable temperature node and heat flux to design a cooling system around. The cooling system must be able to keep the outside of the iPEBB under 109.16 degrees Celsius, and the system must be able to provide a heat sink for a heat source of 1188W. This corresponds to a heat flux of:

$$Q_{sink} = 76.48 \frac{kW}{m^2}$$

The current study provides a first order estimate to calculate a temperature node on the outside of the iPEBB, but a more accurate model would have a heat spreading angle that is tested on the real iPEBB substrate wall.

D. Conclusions

The current study validated many heat transfer assumptions to simplify the complex thermal system within the iPEBB into two main components: the MOSFET rows and the transformer. After analyzing the heat fluxes and thermal resistances of each system, the present study revealed maximum critical temperatures that need to be imposed on the outside wall of the iPEBB in specific areas that directly impact the thermal system of the transformer and the MOSFET rows. Furthermore, the heat flux from both thermal systems is known, and a cooling system can easily be designed around the heat flux and temperature constraints.

Each MOSFET row system produces waste heat of 1188W and leaves the iPEBB wall with a surface area of 0.0155 m² due to the calculated heat spreading effects. This means that the heat sink needed to cool each row would need to dissipate a heat flux of 76.48 kW/m². This surface area has a large degree of uncertainty because it is determined by using a heat spreading angle found from experimentation on a multilayered substrate that is slightly different than the actual iPEBB substrate. The spreading angle of 67.3 degrees is an indicative but not exact representation of the true spreading angle; therefore, the heat flux calculated has significant uncertainty. The outside surface temperature of the iPEBB wall within the affected surface area needs to be below 109.16 degrees Celsius for the MOSFETs to remain below their maximum operating temperature. It is important to note that there is a total of 4 MOSFET rows in the iPEBB, and therefore the final cooling system should be able to meet the requirements specified above for each of the four row locations.

The transformer system produces 428.794W of waste heat through one side of the iPEBB wall and has a surface area of 0.0774 m², leading to a total heat flux of 5.539 kW/m². Moreover, the temperature on the outside wall of the iPEBB that is directly beneath the transformer must be below 223.5 degrees Celsius to keep the transformer under its Curie temperature. This heat flux leaves the iPEBB at the top and bottom surfaces, so a cooling design would need to be placed on both sides of the iPEBB to thoroughly cool the transformer.

Since the heat flux of the MOSFET row is 13.8 times larger than the heat flux leaving the transformer, the MOSFET system will need a far more robust cooling solution. The current study recommends focusing most of the cooling efforts on the MOSFET system over the transformer.

The current study is strictly a first order analytical solution that performs engineering assumptions common in heat transfer to estimate how heat flows within the iPEBB. There was no direct experimentation with components used in the iPEBB, and there was no finite element thermal analysis. Although the results from this study are backed by thermodynamic analysis, the iPEBB needs to be experimentally tested to verify the results of the present study. Notably, the largest area of concern is the heat spreading that occurs from the MOSFET heat source. Since the heat flux is so large, the thermal spreading effects have a large impact on the total resistance of the system. The thermal spreading angle utilized by the current study was not determined through experimentation of the iPEBB substrate wall, and the accuracy of the heat spreading theory could be easily improved through an experiment with the same design as the experiment in section C.a.

Overall, the current study provides a solid understanding of the main modes of heat transfer within the iPEBB and suggests thermodynamic constraints necessary for future design of cooling systems for the iPEBB.

References

- [1] "GE Powers US Navy's 1st Full-electric power and propulsion ship," *GE News*. [Online]. Available: https://www.ge.com/news/press-releases/ge-powers-us-navy%E2%80%99s-1st-full-electric-power-and-propulsion-ship. [Accessed: 26-Mar-2022].
- [2] S. Berry, "Electricity Shifts the Currents of Ship Propulsion," SIGNAL Magazine, 16-Jan-2015. [Online]. Available: https://www.afcea.org/content/?q=electricity-shifts-currents-ship-propulsion#:~:text=The%20U.S.%20Navy%20now%20is%20transitioning%20to%20all-electric,sailors%20into%20harm%E2%80%99s%20way%E2%80%94and%20lowered%20ship%20life-cycle%20costs. [Accessed: 26-Mar-2022].
- [3] L Petersen, C Schegan, T Ericsen, D Boroyevich, R Burgos, N Hingorani, M Steurer, J Chalfant, H Ginn, C DiMarino, G Montanari, F Peng, C Chryssostomidis, CM Cooke, and I Cvetkovic. Power electronic power distribution systems (PEPDS). ESRDC Website, www.esrdc.com, 2022.
- [4] J. del Ferrandis, J. Chalfant, C. M. Cooke, and C. Chryssostomidis, "Design of a Power Corridor Distribution Network," 2019 IEEE Electric Ship Technologies Symposium (ESTS), 2019.
- [5] C. M. Cooke, C. Chryssostomidis, and J. Chalfant, "Modular Integrated Power Corridor," 2017 IEEE Electric Ship Technologies Symposium (ESTS), 2017.
- [6] J. Padilla, J. S. Chalfant, C. Chryssostomidis, and C. M. Cooke, "Preliminary Investigation into Liquid-Cooled Pebbs," 2021 IEEE Electric Ship Technologies Symposium (ESTS), 2021.
- [7] Rajagopal, N. (n.d.). Navy Integrated Power Electronics Building Block (Navy iPEBB). *Electric Ship Research and Development Consortium*.
- [8] Raju, R. (2020). HF Transformer. CPES-Virginia Tech/ONR IPEBB-1000 Program.
- [9] R. E. Simons, "Simple formulas for estimating thermal spreading resistance," Electronics Cooling, 01-May-2004. [Online]. Available: https://www.electronics-cooling.com/2004/05/simple-formulas-for-estimating-thermal-spreading-resistance/. [Accessed: 27-Apr-2022].
- [10] G. N. Ellison, "Maximum thermal spreading resistance for rectangular sources and plates with nonunity aspect ratios," IEEE Transactions on Components and Packaging Technologies, vol. 26, no. 2, pp. 439–454, 2003.
- [11] B. Guenin, "The 45° heat spreading angle an urban legend?," Electronics Cooling, 02-Jul-2019. [Online]. Available: https://www.electronics-cooling.com/2003/11/the-45-heat-spreading-angle-an-urban-legend/?msclkid=9f07d19fc6a411ec813b5b11ec0029c2. [Accessed: 28-Apr-2022]

Appendix

Core Biot analysis:

$$R_{cond,core} = \frac{t_{core}}{K_{iron}A_{c,core}}$$

Where:

$$A_{c,core} = L_{core} * W_{core}$$

$$R_{conv,core} = \frac{1}{h_{core}A_{s,core}}$$

Where:

$$h_{core} = 5 \frac{W}{m^2 K}$$

And:

$$A_{s,core} = t_{core}(L_{core} + W_{core})$$

Solving:

$$Bi_{core} = \frac{R_{cond,core}}{R_{conv,core}} = \frac{0.0172}{24.6125} = 6.9 * 10^{-4}$$

Temperature Profile of Transformer Core:

$$-K_{iron}A_{core}\frac{dT}{dx}\Big|_{x_{core}} + q_{gen}A_{core}dx + K_{iron}A_{core}\frac{dT}{dx}\Big|_{x_{core}+dx} = 0$$
 (1)

Where:

$$K_{iron}\frac{dT}{dx}\mid_{x_{core}=x+dx}=K_{iron}\frac{dT}{dx}+K_{iron}\frac{dT}{dx}(\frac{d}{dx})dx=K_{iron}\frac{dT}{dx}\mid_{x_{core}=x}+K_{iron}\frac{d^2T}{dx^2}dx \quad \ \ (2)$$

Plugging (2) into (1):

$$q_{gen}A_{core}dx + K_{iron}A_{core}\frac{d^2T}{dx^2}dx = 0$$
(3)

$$q_{gen} + K_{iron} \frac{d^2T}{dx^2} = 0$$

$$\frac{-q_{gen}}{K_{iron}}dx^2 = d^2T$$

$$\left[\frac{-q_{gen}}{K_{iron}}x + D_1\right]dx = dT \tag{4}$$

$$\frac{-q_{gen}}{2K_{iron}}x^2 + D_1x + D_2 = T(x_{core})$$
 (5)

Temperature Profile of Transformer Substrate:

$$-K_{sub}A_{core}\frac{dT}{dx}\Big|_{x_{sub}=x} + K_{sub}A_{core}\frac{dT}{dx}\Big|_{x_{sub}=x+dx} = 0$$
 (1)

Where:

$$K_{sub}\frac{dT}{dx}\left|_{x_{sub}=x+dx} = K_{sub}\frac{dT}{dx} + K_{sub}\frac{dT}{dx}(\frac{d}{dx})dx = K_{iron}\frac{dT}{dx}\left|_{x_{sub}=x} + K_{sub}\frac{d^2T}{dx^2}dx\right. \tag{2}$$

Plugging (2) into (1):

$$K_{iron}A_{core}\frac{d^2T}{dx^2}dx = 0 (3)$$

$$\frac{d^2T}{dx^2} = 0\tag{4}$$

Integrating (4):

$$\frac{dT}{dx} = e_1 \tag{5}$$

Integrating (5):

$$T(substrate) = e_1x + e_2 \tag{6}$$